Valorisation of 2,5-dimethylfuran over zeolite catalysts studied by on-line FTIR-MS gas phase analysis

N.B. When citing this work, cite the original published paper.

(article starts on next page)

PAPER

Check for updates

Valorisation of 2,5-dimethylfuran over zeolite catalysts studied by on-line FTIR-MS gas phase analysis†

Christopher Sauer, [iD] *[a] Anders Lorén,[b] Andreas Schaefer [iD] [a] and Per-Anders Carlsson [iD] *[a]

The valorisation of 2,5-dimethylfuran (2,5-dmf) by catalytic fast pyrolysis (CFP) was studied by on-line FTIR-MS gas phase analysis. Zeolite beta, H-ZSM-5 and Cu-ZSM-5 were characterised and used as catalysts. The on-line analysis enables sufficient time resolution to follow subminute transient phenomena, *e.g.*, the impact of catalyst pretreatment and time on stream (TOS) on the reaction selectivity. The results show, that the initial selectivity towards benzene, toluene and xylene (BTX) aromatics is high but decreases with TOS while the isomerisation rates of 2,5-dmf towards 2,4-dimethylfuran and cyclic ketones increase. This indicates the involvement of specific active sites for the different conversion processes. The formation of BTX compounds is linked to the availability of specific olefins, as supported by temperature programmed desorption experiments, which is indicative of aromatisation stemming directly from the olefin pool rather than *via* Diels–Alder reactions.

1 Introduction

The global need to develop our economies by using sustainable resources creates an obvious demand for the chemical industry to implement chemical building blocks made from renewable bio-based materials.[1] Grouped together, the aromatics benzene, toluene and xylenes (BTX) are among the five most important commodity chemicals.[2,3] Unlike many other chemicals, BTX cannot be manufactured directly from syngas, which presents a potentially green route provided the syngas stems from biogas, but needs another feedstock. One possibility is to use furans. Furans can be obtained from wooden biomass such as lignin and (hemi)cellulosic materials[4–6] and thus these furans would not compete with food production nor require specialised crops. The utilization of biomass must of course involve a critical assessment as to achieve sustainable forestry and must also consider the protection of ecosystems and biodiversity.[7–9] Using so-called catalytic fast pyrolysis (CFP), the biomass is rapidly heated to form vapours containing among other constituents furans, which subsequently can be catalytically converted into a number of prod-

ucts with higher value.[10–12] In this connection, predominantly 2,5-dimethylfuran (2,5-dmf) but also other furanics have been used as representative model compounds suitable for synthesis of BTX.

For the catalytic conversion of furans to BTX, MFI and beta type zeolites have been identified as promising catalyst candidates due to their shape selectivity.[13,14] As examples, the selectivity towards BTX has been reported to be 20%,[15] 35%[16] and *ca.* 50%.[17,18] Among the BTX compounds, the *p*-xylene is the product with highest market value because of its use as a precursor for terephthalic acid, the monomor used for PET production.[19]

The selective production of *p*-xylene as well as other compounds in the BTX family has been studied extensively using high-pressure reactors operated in batch mode. With an aliphatic solvent such as *n*-heptane, an ethene pressure of approximately 50 bar and catalysts such as H-BEA, tin phosphate, or others, selective production (≥90%) of *p*-xylene has been demonstrated.[20–22] The reaction has been proposed to proceed through a Diels–Alder cycloaddition with subsequent dehydration (DACD).[3,23] This reaction pathway is highly desirable because it builds on the natural chemical complexity of the 5-membered furan ring so as to produce the 6-membered carbon rings, with the only byproduct being benign water.[3] It has been found that the DA reaction is catalysed by Lewis acid sites (LAS) but not Brønsted acid sites (BAS),[3,24] whereas the dehydration of the bicyclic intermediate, which cannot occur in reasonable rates uncatalysed, is facilitated by

a Department of Chemistry and Chemical Engineering, Chalmers University of Technology, Göteborg, Sweden. E-mail: per-anders.carlsson@chalmers.se; Fax: +46 (0)31 160 062; Tel: +46 (0)31 772 2924
b Department of Chemistry and Materials, RISE Research Institutes of Sweden, Borås, Sweden

† Electronic supplementary information (ESI) available. See DOI: 10.1039/d1cy01312b

both LAS and tremendously by BAS.[24–26] Overall, the route to *p*-xylene *via* DACD is kinetically limited by the cycloaddition over BAS and dehydration on LAS.[22,24,27,28]

Industrial production of commodity chemicals demands continuous processes and the manufacturing of BTX compounds is no exception. In this respect, Mendoza Mesa *et al.* successfully showed that the selective production of *p*-xylene from 2,5-dimethylfuran and acrylic acid is possible using a continuous flow reactor and zeolite beta. The approach, however, is still reliant on high pressure (30 MPa) conditions and a solvent (heptane),[29] which is better avoided according to green chemistry principles.[30] Hence, it is of high interest to explore the selective production of BTX from cellulosic materials or furans (as model compounds) in gas phase and under CFP conditions. Concerning the reaction pathway and the operating mechanism behind 2,5-dmf conversion over zeolites, the common understanding is rather weak compared to many other catalytic reactions.

The aim of this work is thus to clarify several aspects concerning, *e.g.*, the role of zeolite acidity and micro porous structure, deactivation processes of active sites and transient phenomena. Hitherto, on-line spectroscopic analysis methods have not been particularly used to characterise gas streams in this research field. Instead, the product mixture is usually analysed by collection and separation based methods such as GC-MS/FID, with a time resolution ranging typically from 0.05 min^{-1} to 0.16 min^{-1}.[12,17] By using a newly introduced sophisticated method combining on-line Fourier transform infrared (FITR) spectroscopy and ion–molecule-reaction mass spectrometry (IMR-MS), the effluent stream is analysed with a much higher time resolution of 4 min^{-1}.[31] This paves the way for monitoring changes in product distribution over time, and thereby clarify catalyst performance, in contrast to many reported product selectivities and carbon yields to specific products that depend on sampling time.

To meet our aim we systematically evaluate the product formation during conversion of 2,5-dmf over ZSM-5 catalysts with different SiO_2/Al_2O_3 ratio (SAR), as well as a ZSM-5 ion-exchanged with Cu, and make comparisons with that of zeolite beta. On the one hand, by selecting already studied materials, the results by on-line analysis can be compared with previous results obtained with other analysis methods focusing on the significance of continuous operation. On the other hand, by selecting materials, *i.e.*, the Cu-exchanged zeolites, not used for this reaction before, the potential to improve catalyst design can be explored. So have Cu-exchanged zeo-lites already been used for other Diels–Alder cycloaddition reactions.[32] The measurements of global activity and selectivity are complemented by temperature programmed desorption and *in situ* diffuse reflectance infrared Fourier transform spectroscopy (DRIFTS) measurements so as to delve deeper into adsorption–desorption behaviour and mechanistic pathways.

We show that the product distribution is considerably different depending on the catalyst material. The BTX formation seems to correlate with olefin formation, and Cu functionalisation promotes benzene formation at high temperatures. Interestingly, the selectivity towards olefins and aromatics decreases with time on stream, while there is a trend of increasing selectivity towards 2,4-dimethylfuran (2,4-dmf), and 2- and 3-methyl-2-cyclopenten-1-one, likely formed through isomerisation of 2,5-dmf. This observation paves the way for selective production of the aforementioned compounds from 2,5-dmf by catalyst design.

2 Materials and methods

2.1 Catalytic materials and chemicals

Zeolite materials of the type H-BEA (Zeolyst international) and ZSM-5 (AkzoNobel) were used as catalysts. Their characteristics are presented in Table 1. Elemental analyses and determination of the SiO_2/Al_2O_3 ratio (SAR) of the catalyst powders was carried out by X-ray fluorescence (XRF) using a PANalytical AXIOS instrument. The crystal phases of the catalyst samples were analysed by X-ray powder diffraction (XRD) with a Bruker AXS D8 Advance diffractometer with monochromatic Cu-Kα radiation (0.15406 nm) scanning from 5 to 70° 2θ (acquisition time 1 s). Nitrogen isotherms were measured at 77 K using a Micromeritics Tristar 3000 instrument. Prior to the analysis the samples were degassed at 90 °C for 1 h and then 250 °C for ≥6 h (temperature ramp 10 °C min^{-1}).

To perform the catalytic tests *ca.* 160 mg powder sample was deposited on a cordierite monolithic substrate (Corning, 400 cpsi, 188 channels, length = 15 mm, Ø = 13 mm) by a dipcoat process. A slurry was made by mixing the catalyst powder and a binder material (Ludox AS-40 for H-BEA, Sasol Dispersal P2 for ZSM-5) and the monolith substrate was then repeatedly immersed, dried at 200 °C and calcined at *ca.* 500 °C with a heatgun until 200 mg of the mixture was coated onto the substrate.

2,5-dimethylfuran (Sigma-Aldrich, ≥99%), 2,4-dimethyl-furan (ABBlocks, ≥95%), 2-methylfuran (2MF, Sigma-Aldrich,

Table 1 Physico-chemical properties of the catalytic materials used

Sample	SiO_2/Al_2O_3[a]	% Cu[a,b]	SA[c]	S_{micro}[d]	S_{ext}[d]	V_{micro}[d]	Total acidity[e]/mmol g^{-1}	2,5-Dmf adsorbed/mmol g^{-1}
H-ZSM-5(355)	355		433	420	12	0.198	0.300	0.469
H-ZSM-5(38)	38		403	394	9	0.166	0.118	0.156
Cu-ZSM-5(22)	22	2.8	367	348	19	0.140	0.647	0.381
H-BEA(37)	37		648	620	28	0.255	0.230	0.425

[a] Measured by XRF. [b] Further characterisation available.[33] [c] Apparent surface area by BET, p/p_0 = 0.002–0.04 following consistency criteria.[34] [d] By *t*-plot. [e] From NH_3-TPD in mmol g^{-1} catalyst.

99%), furan (Sigma-Aldrich, liquid, 99%), 2-methyl-2-cyclopenten-1-one (Merck/Sigma Aldrich, 98%), 3-methyl-2-cyclopenten-1-one (Merck/Sigma Aldrich, 97%) were used as feedstock and/or calibration purposes.

2.2 Catalytic measurements and on-line analysis

The catalytic tests were carried out in a chemical flow reactor consisting of an insulated quartz tube surrounded by a metal coil for controlled heating using a PID regulator (Eurotherm, Worthing, UK) and K-type thermocouples placed in front and near the catalyst surface. Mass flow controllers (Bronkhorst Hi-Tech, low-ΔP-flow) were used to introduce feed gas mixtures of O_2 and Ar as balance, while liquid reactant was introduced *via* a gas saturator with Ar as carrier gas. The total flow was set to 1500 mL_n min^{-1} resulting in a weighted hourly space velocity (WHSV) of 1.7. WHSV is defined as flow rate of 2,5-dmf divided by the weight of the catalyst, here ≈160 mg. For the on-line analysis the reactor outlet was directly connected to a FTIR gas analyser (MKS MultiGas 2030) and an IMR-mass spectrometer (Airsense Compact, V&F) *via* heated Swagelok connections. The IMR-mass spectrometer was operated with ionising potentials of 10.44 eV (Hg) and 12.13 eV (Xe). A schematic description of the flow reactor setup is given in the ESI† of a previous work.[31]

IR spectra were recorded between 500/600–4000 cm^{-1} with a resolution factor of 0.5 cm^{-1}. The IR spectrometer's optical path length was 5.11 m. The spectra collection and analysis was performed with the MKS MG2000 software suite v.10.2. and FTIR-library v. R3 supplemented with in house calibrations. The software includes a multivariate data analysis tool based on classical least square fitting. The gas concentrations of various compounds are calculated based on their primary analysis band as shown in Table 2. The on-line IR analysis results in a temporal resolution of ≥ 4 min^{-1}.[31]

At the beginning of each experiment a background in Ar at 200 °C was taken. Each catalyst was used in a step-response experiment at the three different steady-state temperatures 300, 400 and 500 °C. The sample was exposed to 2,5-dimethylfuran 90 min durations two times at 500 °C separated by a 30 min Ar period and then one time each at 400 and 300 °C (see also Fig. S1†). Prior to each experiment and after the last 2,5-dmf exposure at each temperature, the catalyst was regenerated under a flow of 20% oxygen (Ar balance) during a heating ramp up to 700 °C to remove carbon species deposited as coke.

Temperature programmed desorption (TPD) experiments with NH_3 and 2,5-dmf were carried out in the above described chemical flow reactor. The catalyst sample was pretreated in O_2 as described above. The sample was then purged in Ar at 150 °C for 1 h. NH_3-TPD: the sample was saturated with NH_3 by exposing it to 470 ppm NH_3 in Ar at 150 °C for 1 h, then purged in Ar for 1 h. This saturation and purge procedure was repeated to ensure a complete saturation with NH_3. NH_3-TPD was recorded during a temperature ramp of 10 °C min^{-1} from 150 °C to 550 °C and a final dwell time of 1 h in Ar at 550 °C.

Table 2 Information about the analysed molecules of the gas stream. The *m/z* values are those used in the MS analysis

Compound	Formula	*m/z*	IR band/cm^{-1}
Other rings			
2-Methylnaphthalene	$C_{11}H_{10}$	142	
Naphthalene	$C_{10}H_8$	128	758.62–807.32
2-Methyl-CPO	C_8H_8O	(96), 68	1668.88–1809.90
3-Methyl-CPO	C_8H_8O	(96), 68	1701.42–1811.83
Furans			
2,5-Dimethylfuran	C_8H_8O	96, (81)	1168.43–1282.69
2,4-Dimethylfuran	C_8H_8O	(96), 68	1074.17–1174.70
2-Methylfuran	C_7H_6O	(81)	1117.57–1176.87
BTX			
Benzene	C_6H_6	78	606.51–726.80
Toluene	C_7H_8	92	689.44–769.95
o-Xylene	C_8H_{10}	106	702.45–779.59
p-Xylene	C_8H_{10}	106	735.32–867.92
Olefins			
Ethene	C_2H_4	(28), 27	900.12–1000.16
Propene	C_3H_6	42, (41)	900.61–1019.69
1,3-Butadiene	C_4H_8	(54), 39	2698.93–2822.36
C1			
Methane	CH_4	—	3000.25–3176.23
Carbonmonoxide	CO	28	2146.16–2159.90
Carbondioxide	CO_2	44	2223.57–2280.94
Formaldehyde	CH_2O	(30)	2698.93–2822.36
Water	H_2O	18	1416.97–1502.31

2,5-Dmf-TPD: the sample was saturated with 2,5-dmf by exposing it to 400 ppm 2,5-dmf in Ar at 150 °C for 30 min, then purged in Ar for 30 min. This saturation and purge procedure was repeated to ensure a complete saturation with 2,5-dmf. In 20% oxygen (Ar balance) TPD of CO, CO_2 and other hydrocarbons according to the on-line analysis was recorded during a temperature ramp of 10 °C min^{-1} from 150 °C to 700 °C followed by a final dwell time of 30 min at 700 °C. For the H-BEA(37) sample the whole procedure was repeated but this time the TPD happened in pure Ar.

2.3 *In situ* infrared spectroscopy

In situ infrared spectroscopy in diffusive reflectance mode (DRIFTS) was carried out using a Bruker Vertex 70 spectrometer equipped with a praying mantis diffuse reflectance accessory and a stainless steel high-temperature reactor cell (Harrick Scientific Products Inc.) with CaF_2 windows. The instrument was equipped with a liquid nitrogen cooled mercury cadmium telluride detector (bandwidth 600 cm^{-1} to 12 000 cm^{-1}). Spectra were measured between 4000 cm^{-1} to 650 cm^{-1} in a resolution of 1 cm^{-1}. Aperture was 4 mm to 6 mm and sensitivity gain ×2 or ×4. The sample was sieved and the fraction 38 μm to 75 μm was used to form the powder bed that was supported by a mesh of stainless steel. The sample was pretreated with 20% O_2 for 1 h at 550 °C before a background spectrum was recorded in pure Ar at 25 °C and 30 °C.

Temperature programmed desorption (TPD) measurements were carried out by first saturating the powdered catalyst. This was done by adding a droplet of 2,5-dmf or exposing it to a 2,5-dmf in Ar stream until the IR-signal did not change any longer. The cell was then flushed with Ar until all gaseous 2,5-dmf was removed. The TPD experiments were carried out in a 100 mL_n min^{-1} Ar flow and step-wise temperature increase from 30 °C to 300 °C or 30 °C to 550 °C with a temperature interval of 10 or 25 °C respectively. Spectra for each step were recorded during steady conditions 5 min after the target temperature was reached. Desorption products were analysed by MS.

3 Results and discussion

We start this section by first commenting on the catalysts characteristics. We then discuss the continuous flow-reactor step-response experiments focusing on the general trends in 2,5-dmf conversion and resulting product selectivity. Thanks to the combined (gas phase) FTIR spectroscopy and IMR-MS,[31] the drastic changes in activity and selectivity of the zeolite catalysts as a function of time on stream (TOS) can be followed by high time resolution (4 min^{-1}). The carbon balance is around 90%. The on-line analysis reveals even small oscillations in the reactant feed (±5% to 7%), which do however not impact the general trends observed for the product formation. The development of absolute concentrations during TOS at the three temperatures 300, 400 and 500 °C are found in Fig. 1 to 3 and Fig. S10 and S11.† We then deepen the discussion by mechanistic interpretations of the flow-reactor results using the results from the temperature programmed desorption measurements and *in situ* DRIFTS characterisation.

3.1 Sample characterisation

The elemental composition of the catalyst samples has been characterised by X-ray fluorescence spectroscopy (XRF) (see ESI† for detailed information). The derived SAR are given in Table 1 and is indicated in the sample label, *e.g.* H-ZSM-5(38). Cu content for the Cu-ZSM-5 sample is 2.8 wt%, which is further characterised in another work.[33] The crystal phases were analysed by powder X-ray diffraction (XRD). The diffractograms are shown in Fig. S3† and exhibit characteristic peaks of the ZSM-5 and BEA structure respectively.[35] N_2-isotherms are depicted in Fig. S4† and all samples show type I isotherms as expected for zeolites. H-ZSM-5(355), Cu-ZSM5(22) and H-BEA(37) show a type II hysteresis associated to capillary condensation. H-ZSM5(38) shows additionally a hysteresis in the lower range of type IV, often found for aggregated crystals of zeolites.[36] The total amount of acid sites of the samples was determined by NH_3-TPD in a temperature range of 150 °C to 550 °C and is summarised in Table 1 (Fig. S5†). H-ZSM-5(355), which has the least amount of aluminium, shows also the lowest amount of acid sites (0.118 mmol g_{Cat}^{-1}) compared to the H-ZSM-5(38) and H-BEA(37) that are richer in aluminium with 0.300 mmol g_{Cat}^{-1} and 0.230 mmol
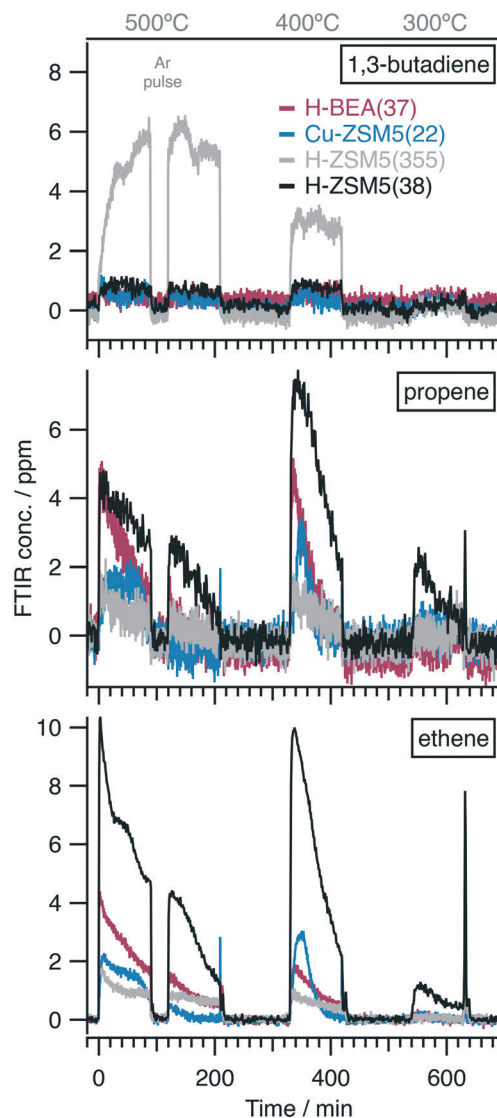

Fig. 1 Concentration profiles of 1,3-butadiene, propene and ethene as determined by on-line FTIR during 2,5-dmf step-response measurements over zeolite catalysts at temperatures 500 °C; 400 °C; 300 °C.

g_{Cat}^{-1} respectively. The Cu-ZSM-5 sample shows the highest value, which is due the fact that the Cu centre can host several NH_3-molecules depending on its oxidation state.[37,38] In addition, 2,5-dimethylfuran TPD experiments were also performed (Fig. S6†). Once adsorbed, a significant part of the 2,5-dmf will not readily desorb as 2,5-dmf from a zeolite. Instead it undergoes reactions, converts to other products, when increasing the temperature. This is for example visible in Fig. 7 and is discussed in detail later. In order to determine the amount of 2,5-dmf adsorbed, we apply the saturated sample to an oxidative treatment during a temperature ramp. This results in the release of "carbon equivalents" mostly in the form of CO and CO_2, but also trace amounts of 2,5-dmf, olefins and BTX. From the signal strength of these carbon equivalents we calculate back how much 2,5-dmf has been adsorbed on the catalyst. The determined amounts are

in the same order of magnitude as the amount of acid sites. Even though the values are slightly higher, they show the same trend, that has been described for the NH$_3$-TPD. One exception is the Cu-ZSM-5 sample, showing a similar value to the H-ZSM-5(38) and H-BEA(37) sample, indicating that Cu does not host several 2,5-dmf molecules as in contrast to NH$_3$. This leads to the assumption that approximately one acid site adsorbs one 2,5-dmf molecule.

3.2 Olefin products

We start off this section by considering olefins, which are some of the main products from catalytic conversion of furanic compounds over zeolites.[15–17] The present focus is on the 1,3-butadiene as well as the two main alkenes, namely, ethene and propene. Although propadiene has been postulated to play a role during aromatisation,[15,16] and also been observed during furan conversion,[15] the presence of propadiene in the product stream during 2,5-dmf conversion cannot be confirmed here.

Looking at Fig. 1, 1,3-butadiene is preferably formed over H-ZSM-5(355) especially at 500 °C, which has the lowest acid site concentration, whereas the three other catalysts only show traces of 1,3-butadiene. Clearly, acidity seems to play a significant role. H-ZSM-5(355) is evidently less acidic due to lower Al content. The lack of acid sites for further conversion (e.g. cracking) of 1,3-butadiene could be an explanation, why H-ZSM-5(355) shows the highest production. Also possible is that 1,3-butadiene is formed by very specific acid sites. The production of 1,3-butadiene is rather constant with TOS in contrast to propene and ethene, which are decreasing with TOS, indicating that that different acid sites must be responsible for the production of ethene and propene in contrast to butadiene. For future studies we suggest the determination the acid sites by NH$_3$-TPD first for the fresh sample, followed by a 2,5-dmf conversion experiment until the propene and ethene production is close to zero and then another subsequent NH$_3$-TPD without intermittent catalyst regeneration. This would reveal the amount and nature of acid sites that are still active and those that have been deactivated may be singled out.

Comparing the four catalysts for absolute values, H-ZSM-5(38) shows the highest production of both propene and ethene followed by the H-BEA(37) sample. As a general trend, the selectivity towards propene appears highest at 400 °C, whereas for ethene it is 500 °C and almost no activity is observed at 300 °C. For all samples the selectivity towards propene and ethene decreases with TOS in contrast to 1,3-butadiene, which is attributed to an increasing deactivation of certain active sites by coke formation as discussed below. Further analysis of the sample spectra and its residual reveals more peaks in the 880 cm^{-1} to 1000 cm^{-1} region indicating some unidentified C=C species for H-ZSM5(355), which are not visible for the Cu-containing sample (Fig. S9†). Only small amounts of ethene and very small amounts of propene were detected. When normalised to the amount of acid sites,

the relative production of propene and ethene is similar for all samples, (but still slightly higher for H-ZSM-5(38)), suggesting a direct dependency of propene and ethene formation on the amount of acid sites (compare Fig. S12†).

3.3 BTX products

The concentration profiles of the desired BTX products are compiled in Fig. 2. Here the signal of xylenes is a summary of o-xylene and p-xylene due to their overall low concentration. For that purpose we also refer to the MS signal of xylenes (m/z 106) that is more accurate at very low concentrations in Fig. S8.† The selectivity towards xylenes is in general very low for CFP of furanic compounds[12,15–18,39] and more research is needed as to understand how to increase their proportion. The highest toluene formation is observed for
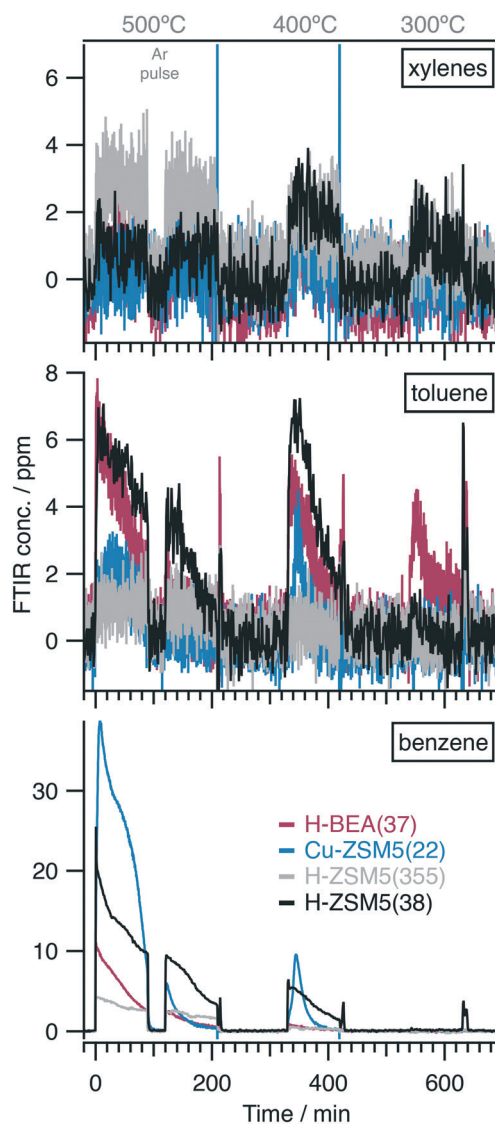

Fig. 2 Concentration profiles of BTX products as determined by on-line FTIR during 2,5-dmf step-response measurements over zeolite catalysts at temperatures 500 °C; 400 °C; 300 °C.

H-ZSM-5(38) and the H-BEA(37) sample at 500 °C and 400 °C. The Cu sample shows significantly higher initial production of benzene, but experiences a faster deactivation compared to H-ZSM-5(38), which shows the second highest selectivity yet slower decline in benzene formation. Firstly, this indicates that benzene formation correlates with the amount of acid sites (Fig. S12†). Secondly, it suggests that the Cu centre might promote benzene formation by being another type of active site. A similar promotion of benzene formation upon metal ion exchange has been found for Ga-ZSM-5.[17] Akin to the here observed selectivity decrease with TOS for the Cu-ZSM-5 sample, Ga-ZSM-5 has been reported to have a shorter catalyst lifetime associated to aromatics.[17]

Benzene is obviously favoured at higher temperature, which was also reported previously using furan[15] and 2,5-dmf[17] as feedstocks. Again, for all samples the BTX selectivity decreases with TOS. The relative signal intensity of propene seems to correlate with that of toluene, while ethene formation seems to correlate with benzene production. This is an indication that aromatics production is dependent on olefins formed directly from 2,5-dmf. The aromatisation could possibly follow a DACD pathway but likely this is not the preferred pathway under CFP conditions,[17] as opposed to those under high pressure in batch reactors, where high selectivity to p-xylene was achieved using unpolar solvents.[20] Instead, the toluene could stem from reactions between two C_2 and one C_3 building blocks, incorporating one propene molecule that contributes with the CH_3 group.

3.4 DMF isomers: 2,4-dimethylfuran

In addition to previous works of 2,5-dmf conversion, the formation of 2,4-dimethylfuran (2,4-dmf) has been observed for all four catalyst samples. 2,4-dmf has been found before as a minor product of wooden biomass conversion[40] and was described to play a role in the decomposition of 2,5-dmf.[41] The presence of this compound was identified by GC-MS and FTIR in our previous work.[31] 2,4-Dmf is a constitutional isomer to 2,5-dmf. Hence a bond break is necessary for the isomerisation. We suggest that the methyl-shift is caused by a combined effect of the BAS and the shape selectivity of the zeolite catalyst. This phenomenon is known for example for the isomerisation of m-xylene to p-xylene in ZSM-5.[42] In Fig. 3 the concentration profile of 2,4-dmf is shown. The selectivity is approximately highest at 400 °C for all samples. For H-ZSM-5(355) and H-ZSM-5(38) the concentration increases with time on stream. This indicates that coking of the catalyst and thus blocking of external sites increases selectivity. The isomerisation is expected to appear in the zeolite pores, which is why MFI structured zeolites are used for isomerisation of xylenes, in good agreement with our observation here based on 2,4-dmf and MFI type ZSM-5. Due to the larger pore size of zeolite beta and thus the lower sterical pressure the selectivity towards 2,4-dmf is lower. Also, the Cu-sample shows a lower selectivity probably due to Cu blocking important BAS isomerisation sites and decreased
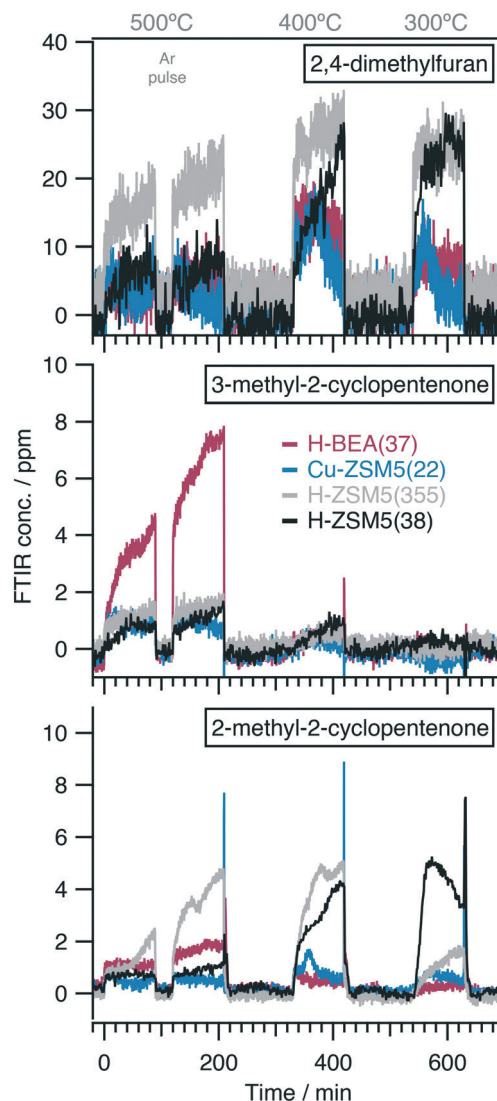

Fig. 3 Concentration profiles of 2,4-dimethylfuran, 3-methyl-2-cyclopenten-1-one and 2-methyl-2-cyclopenten-1-one as determined by on-line FTIR during 2,5-dmf step-response measurements over zeolite catalysts at temperatures 500 °C; 400 °C; 300 °C.

overall acidity. This observation opens the potential for more selective production of the not easily accessible 2,4-dmf from cheap 2,5-dmf. Furthermore, demethylation to 2-methylfuran and methylation to 2,3,5-trimethylfuran has been observed.[31] Similarly, the methylation of furan to 2-methylfuran was reported by Gilbert et al.[43]

3.5 DMF isomers: 2- and 3-methyl-2-cyclopenten-1-one

Two more constitutional isomers have been identified, namely 2- and 3-methyl-2-cyclopenten-1-one. None of these have been previously described during CFP of 2,5-dmf, but 3-methyl-2-cyclopenten-1-one has been observed during 2,5-dmf to p-xylene conversion in the solvated phase,[44] whereas 2-methyl-2-cyclopenten-1-one in the CFP of agricultural waste[40] and other pyrolysis vapours.[45–47] The zeolite

beta sample shows the highest selectivity towards 3-methyl-2-cyclopenten-1-one at 500 °C, while not much of this product is observed at lower temperatures. ZSM-5 samples seem to favour 2-methyl-2-cyclopenten-1-one, with H-ZSM-5(355) showing highest selectivity at 400 °C and H-ZSM-5(38) at 300 °C. The Cu functionalised sample shows lower selectivity, which can be explained by Cu suppressing the ketone formation by blocking important active sites. In other studies 3-methyl-2-cyclopenten-1-one has been observed as a side product when 2,5-dmf is converted in the solvated phase *e.g. n*-heptane. This was explained by initial formation of 2,5-hexanedione by hydrolysing 2,5-dimethylfuran and subsequent dehydration and intra molecular aldol condensation to 3-methyl-2-cyclopentenone.[48,49] The cyclisation is dependent on the availability of acid or basic sites and the SAR. For example it is reported, that calcined, basic forms of high silica Na-containing ZSM-5 favour the cyclisation to the methyl cyclopentenone, whereas acidic H-ZSM-5 favour 2,5-dimethylfuran as illustrated in Fig. 4.[50,51] It is suggested to be used diagnostically to determine the presence of basic sites in zeolitic catalysts.[51]

Also the selective production of 3-methylcyclopenten-1-one from 2,5-dmf *via* 2,5-hexanedione (hydration and subsequent intra aldolcondensation) has been described. The reaction of 2,5-hexanedione *via* dehydration back to 2,5-dmf was found to be competing and favoured.[52] However, in this work the presence of 2,5-hexanedione in the gas phase can not be confirmed. A possible explanation is the absence of the solvent and the difference in pressure (50 bar *vs.* atmospheric) and temperature (250 *vs.* ≥300 °C), which does not allow desorption of 2,5-hexanedione. Further, water might desorb faster and is thus not available for the hydrolysis reaction of 2,5-dmf. Instead, hydrolysis might occur by zeolitic hydroxyl groups, which do not allow desorption to 2,5-hexanedione under these conditions remaining as one possibility for the isomerisation of 2,5-dmf to 3-methyl-2-cyclopenten-1-one. Accordingly, 2,4-dmf could thus be considered being rearranged to 2-methyl-2-cyclopenten-1-one. BAS assisted methyl shift from 3- to 2-methyl-2-cyclopenten-1-one and *vice versa* could be an alternative pathway.
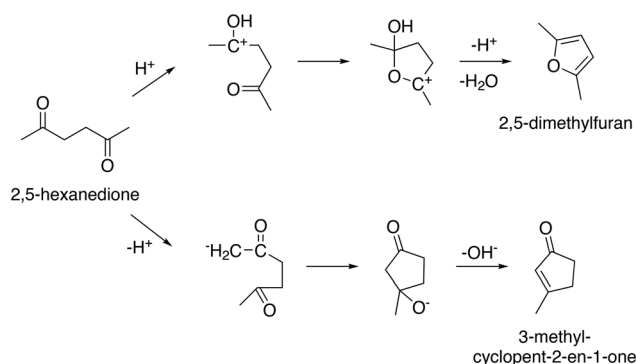

Fig. 4 Proposed mechanism for zeolite catalysed cyclisation of 2,5-hexanedione to 2,5-dimethylfuran and 3-methyl-cyclopent-2-en-1-one.[51]

Further conversion products that were studied include methane, which is mostly produced at 500 °C, but lesser amounts are even detectable at lower temperatures. H-BEA(37) has the highest selectivity, followed by the Cu-ZSM-5(22) and H-ZSM-5(355). The lowest methane production is observed with H-ZSM-5(38). Formaldehyde was detected during the oxidative regeneration of the catalyst. Under the conditions (20% oxygen) complete oxidation of coke species to CO_2 and H_2O seems difficult as even shown by the presence of CO during ox. regeneration (Fig. S10†). Furthermore, the studied catalyst samples show differences in selectivity towards CO, CO_2 and H_2O even during the conversion of 2,5-dmf. Uslamin *et al.* found that unsubstituted furan undergoes decarbonylation to CO_x, while methylated furans are deoxygenated by dehydration.[17] In this study we observe that selectivity to CO, CO_2 and H_2O decreases with temperature which is related to lower 2,5-dmf conversion. The beta sample seems to facilitate dehydration over decarbonylation showing the lowest selectivity trend towards CO_x. H-ZSM-5 samples both show higher decarbonylation activity. The Cu-ZSM-5 has very high initial CO_x production at all temperatures which quickly declines. For this sample it is found that CO_x is favoured during the first minutes of the conversion, while hydrocarbons show peak formation after the (rapid) decline of the CO_x signal which is discussed in more detail below.

3.6 Mechanistic insights

The activity and selectivity stem from the interaction of 2,5-dmf and its conversion products with the active sites in the zeolite. These interactions are not straightforward to resolve completely. Temperature programmed desorption and *in situ* infrared spectroscopy, however, are two appropriate techniques that can shine light on some products and surface species resulting from the chemical transformations and that may be important in the reaction mechanism(s). Here we discuss desorption by mass spectrometry and preoxidation as well as evolution of surface species by *in situ* IR.

3.6.1 Effect of preoxidation of Cu. Referring back to the high initial CO_x production for the Cu-ZSM-5 sample we observed a delayed maximum formation of BTX and olefins compared to the H-form zeolite samples. Fig. 5 shows the CO and CO_2 signal together with BTX and olefins. Obviously, CO_x production is favoured in the first minutes upon exposure to 2,5-dmf, while hydrocarbons experience their maximum after the rapid decline of CO_x. This observation is explained by the preoxidation of Cu-species during the oxidative treatment, where Cu-centres function as oxygen storage. That means, the pre oxidised Cu-species in the zeolite can act as an oxidation catalyst of the carbon-rich reactant.[53]

During temperature programmed *in situ* IR experiments a pronounced band is found at 2156 cm^{-1} as displayed in Fig. 6. This band is recorded for temperatures ≥180 °C and assigned to C═O stretching vibrations from CO on Cu-
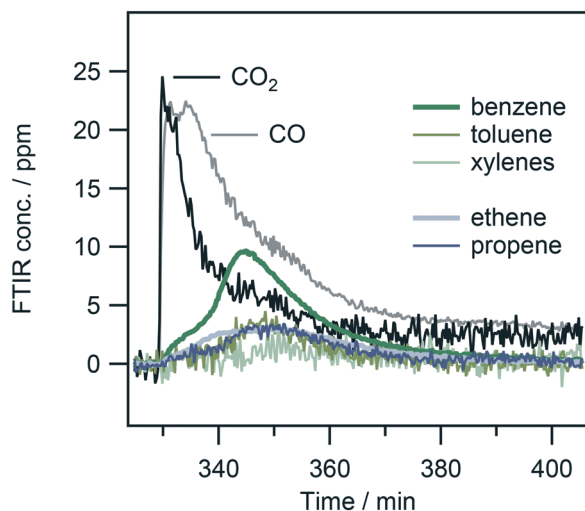
Fig. 5 Concentration profiles of CO and CO_2 together with BTX, ethene and propene for the Cu-ZMS-5 sample during 2,5-dimethylfuran exposure at 400 °C.

species $\nu[Cu^+–CO]$.[33,54] This band supports evidence of the above mentioned decarbonylation pathway of 2,5-dmf.[17] Future studies could examine the role of oxidised *vs.* reduced Cu species, *e.g.*, by hydrogen pre-treatment.

3.6.2 Desorption products from preadsorbed 2,5-dmf. Another aspect investigated concerns the origin of BTX formation. In contrast to previous studies, where 1,2-propadiene has been postulated to play a role during aromatisation,[15,16] the presence of 1,2-propadiene can not be confirmed based on the IR spectra during the on-line analysis. Additionally, the pathway of BTX formation *via* Diels–Alder cycloaddition and subsequent dehydration of furans and olefins in flow reactor conditions is debated.[15,18] Olefins such as ethene and propene directly formed from the furan species can be considered the primary origin of BTX aromatics.[55] To broaden understanding of how 2,5-dmf is transformed upon adsorp-

tion and how olefin and BTX formation are related temperature programmed desorption experiments were carried out.

Beside *in situ* IR for the analysis of surface species, mass spectrometry was chosen to track desorption products as the suitable technique because of the very low analyte concentrations. As shown in Fig. 7, two main regimes are distinguished. The desorption signals below 100 °C are assigned to unreacted 2,5-dmf. Above this temperature no signal of 2,5-dmf is detected. This means that the remaining species are so strongly adsorbed that transformation to other reaction products is favoured over further desorption from the zeolite. At higher temperatures, the desorption of olefins and BTX is recorded. The maximum of the desorption profile for each species was evaluated to obtain the temperature of maximum desorption as summarised in Table 3. In this experiment, the desorption of a C_4H_8 species, assigned to butene, is detected at a similar temperature as xylene around 350 °C. The toluene signal correlates with propene around 380 °C. The desorption maximum of benzene and ethene is found at the highest temperatures, 418 °C and 429 °C respectively. A similar correlation of olefin and BTX formation is also found during the above described on-line IR analysis. This leads to the assumption that C_4 building blocks are incorporated into xylene, C_3 into toluene and C_2 mainly into benzene molecules. When a similar TPD experiment was performed in the continuous flow reactor and desorption products were analysed by FTIR, the same trend correlations are observed, but the absolute temperatures of max. Desorption are somewhat higher. This is probably due to differences in the reactor setup and the experimental procedure, *e.g.* powder sample *vs.* monolith, adsorption temperature (25 °C *vs.* 150 °C), but also due to a rather large error (*ca.* ±15 °C) when detecting these very low concentrations. The results are summarised in Table 3, column B and shown in Fig. S7.†

3.6.3 Surface species. Here we used *in situ* DRIFTS to study surface species upon adsorption of 2,5-dmf to the zeolite. The strong C–O–C-stretch vibration band at 1630 cm^{-1} of gaseous 2,5-dmf is not detected when adsorbed on the zeolite. Instead strong bands at higher wavenumbers are found between 1703 cm^{-1} to 1726 cm^{-1} (Fig. S13 and S15†). The C=O stretch vibration of ketones in gas phase are expected between 1750 cm^{-1} to 1730 cm^{-1}. For example, 2,5-hexanedione shows a strong band at 1734 cm^{-1} and 3-methyl-CPO at 1742 cm^{-1}. On a zeolite however, interaction with BAS leads to a weakening of the C=O bond to about 1710 cm^{-1}.[56–59] Moreover, such interaction between ketone species and Cu is stronger, leading to even weaker C=O bond strength and thus lower frequencies at around 1680 cm^{-1} to 1690 cm^{-1},[56] which can be compared to the observation of the band at 1684 cm^{-1} made here with the Cu-ZSM5(22) sample (Fig. S14†). This band is especially strong at low temperatures and decreases in intensity upon heating. After disappearance of the ketone band above 150 °C a new band at 2156 cm^{-1} for the Cu-sample is observed from ≥160 °C (compare Fig. 6 and S14†), suggesting the conversion of the ketonic C=O stretch vibration to a Cu-carbonyl species with a stronger C=O bond
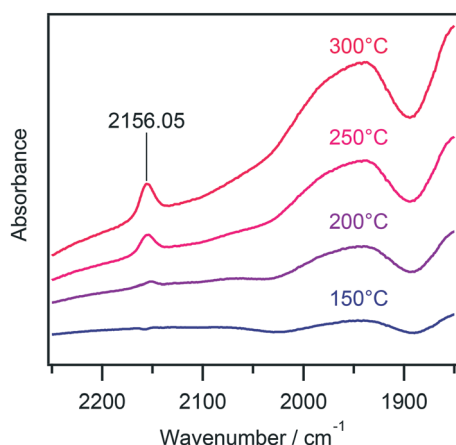

Fig. 6 Background substracted DRIFT spectra showing a band at 2156 cm^{-1} assigned to C=O stretch vibration on Cu during TPD of 2,5-dmf from Cu-ZSM-5(22).
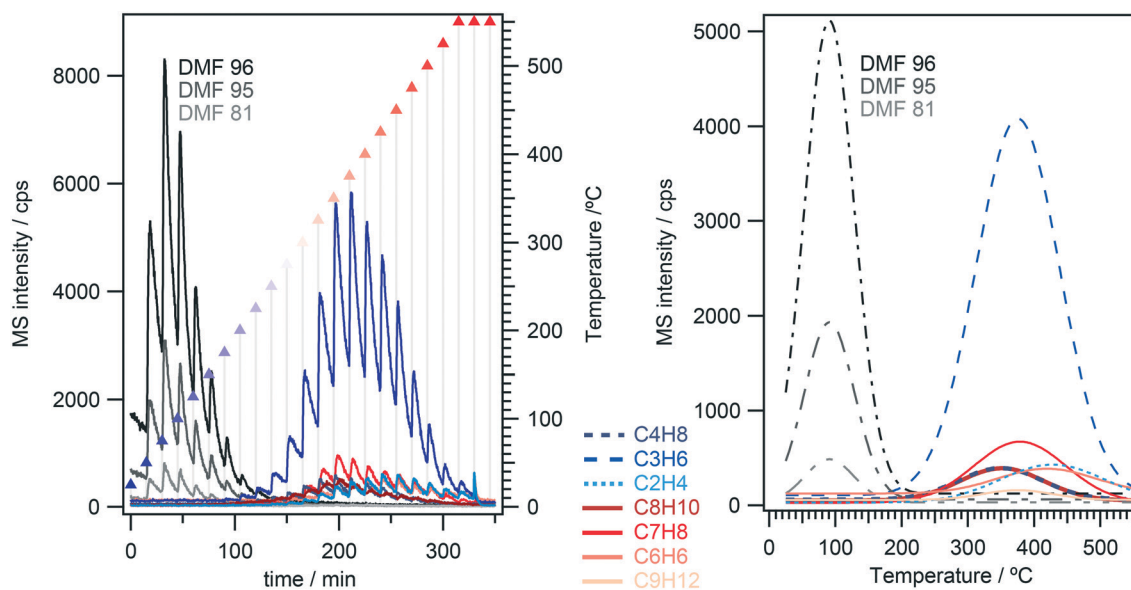
Fig. 7 Temperature programmed desorption of 2,5-dimethylfuran using H-BEA SAR38. Left: MS signal assigned to various olefins and aromatics during the step wise temperature increase. Right: Gaussian fit of the MS signal *vs.* temperature.

(ν[Cu⁺–CO]).[33,54] This indicates that, upon adsorption, 2,5-dmf undergoes a transformation to a species with a carbonyl like vibration interacting with BAS or LAS. This band disappears after heating up to 200 °C, suggesting that some of this species is reverted to 2,5-dmf, which is desorbed and detected by MS as in Fig. 7. Remaining 2,5-dmf/ketone species, that are strongly bound however, are eliminated at higher temperature, forming olefins and CO through decarbonylation. This is indicated by the detection of the Cu-carbonyl signal and the evolution of new bands in the C–H and C≡C stretch vibration region (Fig. S14†) at elevated temperatures. Further support are the bands around 1700 cm⁻¹, which are decreasing in intensity, while no more desorption of 2,5-dmf is detected by MS.

The interaction between the reactant and the acid sites is also indicated by the detection of bands in the O–H-

stretching region. In the case the H-BEA sample (Fig. 8), the peak centred at around 3733 cm⁻¹ is attributed to internal silanols. Visible for all samples, the peaks at around 3746 cm⁻¹ and 3742 cm⁻¹ are assigned to external silanols.[60,61] The first is observed especially at low temperatures and reduces in intensity upon heating so that the signals for the external silanol are revealed.

Further, the band at 3612 cm⁻¹ is assigned to strongly acidic bridged hydroxyl groups (BAS).[62] This peak appears negative in intensity for the H-BEA sample after adsorption. The O–H vibration is observed less strong due to

Table 3 Desorption maxima of 2,5-dmf, aromatics and olefins using H-BEA(37) determined in two different experiments A and B

| Species | m/z/amu | T of max. desorption/°C | |
		A[a]	B[b]
2,5-Dmf	96, 95, 81	91	258
Naphthalene			492
Trimethylbenzene	120	376	
Xylene	106	352	321
Toluene	92	379	392, 453
Benzene	78	418	467
Butene	58	349	
Propene	42	376	387
Ethene	28	429	476
Methane			505

[a] From *in situ* IR experiment, Fig. 7, determined by MS. [b] From Fig. S7† determined by FTIR, (*ca.* ±15 °C).
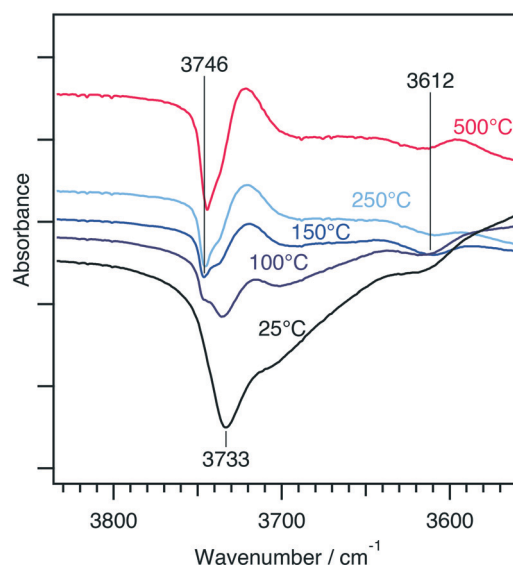

Fig. 8 Background substracted DRIFT spectra of the OH-stretch vibration region showing interaction of the adsorbent 2,5-dmf with terminal silanols and acid sites of H-BEA.

Paper

interaction with the reactant. For the Cu-sample however, no such strong BAS interaction can be observed (Fig. S14†). Instead the signal is positive at low temperatures, indicating that more O–H vibration is observed upon adsorption of 2,5-dmf than before. One explanation is that acid sites were protonated by 2,5-dmf, which itself interacts with the Cu-sites. In contrast, H-ZSM5 shows a strong negative band at 3611 cm^{-1} indicating interaction of the adsorbent with BAS.

Many changes in the C–H stretching region for all samples are observed (Fig. S13 to S15†). The bands between 3000 cm^{-1} to 2900 cm^{-1} are assigned to aliphatic C–H stretching vibrations, whereas the bands 3200 cm^{-1} to 3000 cm^{-1} are assigned to aromatic and olefinic C–H stretch vibrations.[63] One example is the band at 3120 cm^{-1} for the H-BEA(37) sample, which appears in the temperature range of 100 °C to 350 °C. The appearance of bands around 3300 cm^{-1} indicates the presence of alkynyl–C–H vibrations. Highly unsaturated hydrocarbons such as polycycles are also suggested by the broad band around 1580 cm^{-1} formed at high temperatures.[17] This is supported by the black colour of the sample after reaching high temperatures, supporting the formation of soot (highly unsaturated carbon species). A small band between 1479 cm^{-1} to 1471 cm^{-1} is observed for the Cu-ZSM-5 sample. This signal can be assigned to a CC-stretch vibration of benzene in a zeolite. When Cu is present this band is shifted to lower wavenumber.[64] The broadening of the this band in our Cu-sample indicates at least partial benzene or aromatic – Cu interaction. Further CC stretch vibrations between 1580 cm^{-1} to 1510 cm^{-1} are expected to originate from furanic and aromatic species.[17,57]

The band at 1655 cm^{-1} can be attributed to δ_{HOH} bending of water.[33,63] In summary, there are indications that 2,5-dmf is transformed to ketonic species upon adsorption onto the zeolite making DACD impossible under the studied (CFP) conditions. This transformation is however reversible and thus exploited in DACD reactions from 2,5-dmf to *p*-xylene in batch reactor experiments operating at high pressures (*ca.* 50 bar) and long reaction times.[20] In contrast, the aromatisation under CFP conditions is expected to originate solely from the olefin pool, which itself stems from 2,5-dmf through dehydration, decarbonylation and cracking reactions.[17]

4 Conclusions

The valorisation of 2,5-dimethylfuran over Cu- and H-ZSM-5 and beta zeolite has been studied in a continuous flow reactor under CFP conditions. During catalytic step-response experiments, the composition of the effluent gas stream has been analysed by on-line analysis using Fourier transform infrared spectroscopy and ion molecule reaction mass spectrometry. The high time resolution allows the observation of transient phenomena on the product stream such as the influence of pre oxidised Cu-species. We find that initial selectivity to olefins and BTX is high, but decreases with time on stream, which is linked to the deactivation of certain acid sites. With increasing TOS, 2,5-dimethylfuran is isomerised to 2,4-dimethylfuran, 2- and 3-methyl-2-cyclopenten-1-one instead. High acid site concentration is beneficial for olefin and BTX production, but we also find that promoting the ZSM-5 zeolite with Cu-ions can increase initial selectivity towards benzene. Upon adsorption of 2,5-dimethylfuran onto the zeolite, the formation of ketonic species is revealed as well as the formation of CO_x, water and olefins. The formation of BTX correlates with the availability of specific olefins, which is supported by temperature programmed desorption experiments. The aromatisation under CFP conditions is thus expected to originate solely from the olefin pool and not from Diels–Alder-like reactions. It can be concluded that a combination of advanced analysis methods, such as on-line monitoring and *in situ* experiments are necessary to understand the complexity of product distribution and reaction mechanisms. A further study is required to understand which acid sites are responsible for the formation of certain products.

Conflicts of interest

There are no conflicts to declare.

Acknowledgements

References

1 R. A. Sheldon, *Green Chem.*, 2014, **16**, 950–963.

2 A. M. Niziolek, O. Onel, Y. A. Guzman and C. A. Floudas, *Energy Fuels*, 2016, **30**, 4970–4998.

3 A. E. Settle, L. Berstis, N. A. Rorrer, Y. Roman-Leshkóv, G. T. Beckham, R. M. Richards and D. R. Vardon, *Green Chem.*, 2017, **19**, 3468–3492.

4 G. W. Huber, S. Iborra and A. Corma, *Chem. Rev.*, 2006, **106**, 4044–4098.

5 Y. Román-Leshkov, J. N. Chheda and J. A. Dumesic, *Science*, 2006, **312**, 1933.

6 G.-H. Wang, J. Hilgert, F. H. Richter, F. Wang, H.-J. Bongard, B. Spliethoff, C. Weidenthaler and F. Schüth, *Nat. Mater.*, 2014, **13**, 293–300.

7 L. Persha, A. Agrawal and A. Chhatre, *Science*, 2011, **331**, 1606–1608.

8 S. Fares, G. S. Mugnozza, P. Corona and M. Palahí, *Nature*, 2015, **519**, 407–409.

9 R. Hajjar, J. A. Oldekop, P. Cronkleton, P. Newton, A. J. M. Russell and W. Zhou, *Nature Sustainability*, 2020, **4**, 216–224.

10 G. W. Huber and A. Corma, *Angew. Chem., Int. Ed.*, 2007, **46**, 7184–7201.

11 T. R. Carlson, T. P. Vispute and G. W. Huber, *ChemSusChem*, 2008, **1**, 397–400.

12 Y. T. Cheng and G. W. Huber, *ACS Catal.*, 2011, **1**, 611–628.

13 W. W. Kaeding, C. Chu, L. B. Young and S. A. Butter, *J. Catal.*, 1981, **69**, 392–398.

14 J. Jae, G. A. Tompsett, A. J. Foster, K. D. Hammond, S. M. Auerbach, R. F. Lobo and G. W. Huber, *J. Catal.*, 2011, **279**, 257–268.

15 Y. T. Cheng and G. W. Huber, *Green Chem.*, 2012, **14**, 3114–3125.

16 J. S. Espindola, C. J. Gilbert, O. W. Perez-Lopez, J. O. Trierweiler and G. W. Huber, *Fuel Process. Technol.*, 2020, **201**, 106319.

17 E. A. Uslamin, N. A. Kosinov, E. A. Pidko and E. J. M. Hensen, *Green Chem.*, 2018, **20**, 3818–3827.

18 E. A. Uslamin, B. Luna-Murillo, N. Kosinov, P. C. Bruijnincx, E. A. Pidko, B. M. Weckhuysen and E. J. Hensen, *Chem. Eng. Sci.*, 2019, **198**, 305–316.

19 A. Maneffa, P. Priecel and J. A. Lopez-Sanchez, *ChemSusChem*, 2016, **9**, 2736–2748.

20 C.-C. Chang, S. K. Green, C. L. Williams, P. J. Dauenhauer and W. Fan, *Green Chem.*, 2014, **16**, 585–588.

21 X. Feng, Z. Cui, K. Ji, C. Shen and T. Tan, *Appl. Catal., B*, 2019, **259**, 118108.

22 S. Dutta and N. S. Bhat, *Biomass Convers. Biorefin.*, 2020, DOI: 10.1007/s13399-020-01042-z.

23 S. K. Green, R. E. Patet, N. Nikbin, C. L. Williams, C. C. Chang, J. Yu, R. J. Gorte, S. Caratzoulas, W. Fan, D. G. Vlachos and P. J. Dauenhauer, *Appl. Catal., B*, 2016, **180**, 487–496.

24 N. Nikbin, P. T. Do, S. Caratzoulas, R. F. Lobo, P. J. Dauenhauer and D. G. Vlachos, *J. Catal.*, 2013, **297**, 35–43.

25 E. Mahmoud, D. A. Watson and R. F. Lobo, *Green Chem.*, 2014, **16**, 167–175.

26 T. Salavati-fard, S. Caratzoulas, R. F. Lobo and D. J. Doren, *ACS Catal.*, 2017, **7**, 2240–2246.

27 N. J. Abreu, H. Valdés, C. A. Zaror, F. Azzolina-Jury and M. F. Meléndrez, *Microporous Mesoporous Mater.*, 2019, **274**, 138–148.

28 R. E. Patet, N. Nikbin, C. L. Williams, S. K. Green, C.-C. C. Chang, W. Fan, S. Caratzoulas, P. J. Dauenhauer and D. G. Vlachos, *ACS Catal.*, 2015, **5**, 2367–2375.

29 J. A. Mendoza Mesa, F. Brandi, I. Shekova, M. Antonietti and M. Al-Naji, *Green Chem.*, 2020, **22**, 7398–7405.

30 S. L. Tang, R. L. Smith and M. Poliakoff, *Green Chem.*, 2005, **7**, 761–762.

31 C. Sauer, A. Lorén, A. Schaefer and P.-A. Carlsson, *Anal. Chem.*, 2021, **93**, 13187–13195.

32 R. Piffer, H. Förster and W. Niemann, *Catal. Today*, 1991, **8**, 491–500.

33 X. Wang, A. A. Arvidsson, M. O. Cichocka, X. Zou, N. M. Martin, J. Nilsson, S. Carlson, J. Gustafson, M. Skoglundh, A. Hellman and P. A. Carlsson, *J. Phys. Chem. C*, 2017, **121**, 27389–27398.

34 J. Rouquerol, P. Llewellyn and F. Rouquerol, *Stud. Surf. Sci. Catal.*, 2007, **160**, 49–56.

35 C. Baerlocher and L. McCusker, Database of Zeolite Structures, http://www.iza-structure.org/databases/1804.

36 M. Thommes, K. Kaneko, A. V. Neimark, J. P. Olivier, F. Rodriguez-Reinoso, J. Rouquerol and K. S. Sing, *Pure Appl. Chem.*, 2015, **87**, 1051–1069.

37 S. A. Yashnik and Z. R. Ismagilov, *Appl. Catal., A*, 2021, **615**, 118054.

38 L. Chen, T. V. W. Janssens, M. Skoglundh and H. Grönbeck, *Top. Catal.*, 2019, **62**(1), 93–99.

39 Y.-T. Cheng, J. Jae, J. Shi, W. Fan and G. W. Huber, *Am. Ethnol.*, 2012, **124**, 1416–1419.

40 H. Fan, X. Chang, J. Wang and Z. Zhang, *Waste Manage. Res.*, 2020, **38**, 78–87.

41 B. Sirjean and R. Fournet, *Phys. Chem. Chem. Phys.*, 2013, **15**, 596–611.

42 J. Čejka, A. Corma and S. Zones, *Zeolites and Catalysis: Synthesis, Reactions and Applications*, Wiley-VCH, 2010, vol. 1–2.

43 C. J. Gilbert, J. S. Espindola, W. C. Conner, J. O. Trierweiler and G. W. Huber, *ChemCatChem*, 2014, **6**, 2497–2500.

44 J. Yin, C. Shen, X. Feng, K. Ji and L. Du, *ACS Sustainable Chem. Eng.*, 2018, **6**, 1891–1899.

45 D. Wang, C. M. Osmundsen, E. Taarning and J. A. Dumesic, *ChemCatChem*, 2013, **5**, 2044–2050.

46 W. Wang, Y. Shi, Y. Cui and X. Li, *J. Anal. Appl. Pyrolysis*, 2018, **131**, 93–100.

47 Q. Lu, Z.-F. Zhang, C.-Q. Dong and X.-F. Zhu, *Energies*, 2010, **3**, 1805–1820.

48 J. McGlone, P. Priecel, L. Da Vià, L. Majdal and J. Lopez-Sanchez, *Catalysts*, 2018, **8**, 253.

49 C.-C. Chang, H. Je Cho, J. Yu, R. J. Gorte, J. Gulbinski, P. Dauenhauer and W. Fan, *Green Chem.*, 2016, **18**, 1368–1376.

50 V. Calvino-Casilda, R. Martin-Aranda, I. Sobczak and M. Ziolek, *Appl. Catal., A*, 2006, **303**, 121–130.

51 R. M. Dessau, *Zeolites*, 1990, **10**, 205–206.

52 S. Nishimura, S. Ohmatsu and K. Ebitani, *Fuel Process. Technol.*, 2019, **196**, 106185.

53 M. A. Newton, A. J. Knorpp, V. L. Sushkevich, D. Palagin and J. A. Van Bokhoven, *Chem. Soc. Rev.*, 2020, **49**, 1449–1486.

54 J. Engeldinger, C. Domke, M. Richter and U. Bentrup, *Appl. Catal., A*, 2010, **382**, 303–311.

55 E. A. Uslamin, H. Saito, N. Kosinov, E. Pidko, Y. Sekine and E. J. M. Hensen, *Catal. Sci. Technol.*, 2020, **10**, 2774–2785.

56 M. Renz, T. Blasco, A. Corma, V. Fornés, R. Jensen and L. Nemeth, *Chem. – Eur. J.*, 2002, **8**, 4708–4717.

57 L. Kubelková, J. Čejka and J. Nováková, *Zeolites*, 1991, **11**, 48–53.

58 S. Bordiga, C. Lamberti, F. Bonino, A. Travert and F. Thibault-Starzyk, *Chem. Soc. Rev.*, 2015, **44**, 7262–7341.

59 P. Müller, S. P. Burt, A. M. Love, W. P. McDermott, P. Wolf and I. Hermans, *ACS Catal.*, 2016, **6**, 6823–6832.

60 I. Kiricsi, C. Flego, G. Pazzuconi, W. O. J. Parker, R. Millini, C. Perego and G. Bellussi, *J. Phys. Chem.*, 1994, **98**, 4627–4634.

61 D. M. Roberge, H. Hausmann and W. F. Hölderich, *Phys. Chem. Chem. Phys.*, 2002, **4**, 3128–3135.

62 A. A. Gabrienko, I. G. Danilova, S. S. Arzumanov, A. V. Toktarev, D. Freude and A. G. Stepanov, *Microporous Mesoporous Mater.*, 2010, **131**, 210–216.

63 A. S. Rodionov, G. N. Shirobokova, G. N. Bondarenko, Y. V. Pavlyuk, N. V. Kolesnichenko, T. I. Batova, E. N. Khivrich and S. N. Khadzhiev, *Pet. Chem.*, 2013, **53**, 316–321.

64 T. Archipov, S. Santra, A. B. Ene, H. Stoll, G. Rauhut and E. Roduner, *J. Phys. Chem. C*, 2009, **113**, 4107–4116.